[51]Unpublished DESY results.
[52]K. Codling and R. P. Madden, Phys. Rev. Lett. **12**, 106 (1964).
[53]K. Codling, R. P. Madden, and D. L. Ederer, Phys. Rev. **155**, 26 (1967).
[54]A. I. Kozlenkov, Izv. Akad. Nauk SSSR 25, 957 (1961)[Bull. Acad. Sci. USSR Phys. Ser. 25, 989 (1961)].
[55]R. Kronig, Z. Phys. **70**, 317 (1931); Z. Phys. **75**, 191 (1932).
[56]Y. Onodera and Y. Toyozawa, J. Phys. Soc. Jap. **24**, 341 (1968).
[57]K. Codling and R. P. Madden, Appl. Opt. **4**, 1431 (1965).

PHYSICAL REVIEW B VOLUME 7, NUMBER 4 15 FEBRUARY 1973

Quantum-Mechanical Calculations of the Infrared Properties of H^- Ions in Potassium Halides*

R. F. Wood
Solid State Division, Oak Ridge National Laboratory, Oak Ridge, Tennessee 37830
and
B. N. Ganguly
Department of Physics and Materials Research Laboratory, University of Illinois, Urbana, Illinois 61801
(Received 19 June 1972)

The infrared properties of the H^- ion in KCl, KBr, and KI are studied using force constants obtained from quantum-mechanical calculations of the electronic structure of the U center. The anharmonic sidebands of the H^- local mode and the induced far-infrared absorption are calculated. In most cases the calculated force-constant changes give results comparable to the parametrized values used in previous work. It is emphasized that the force-constant changes in A_{1g}, E_g, and T_{1u} displacements are not generally equal. Occasionally, features not found in previously published experimental or theoretical work are observed. Repulsive Born–Mayer potentials for the H^--K^+ interaction in the three crystals are extracted from the quantum-mechanical calculations. Our techniques for handling the numerical evaluation of Green's functions are discussed briefly.

I. INTRODUCTION

Substitutional H^- ions (U centers) in alkali halide crystals have both ultraviolet[1] and infrared[2] absorption bands associated with them. The vibrational properties of crystals containing U centers have proved to be especially interesting. The H^- ion oscillates in a localized mode at a frequency well above that of the highest in-band mode. Sidebands[2,3] containing pronounced structure accompany the local-mode absorption. Since the H^- ions destroy the translational invariance of the host crystal, absorption also occurs in the in-band region of the spectrum.[4] Because of the light mass of H^- compared with the negative ions of the host crystal, the U center was quickly recognized as an interesting system on which to test various aspects of the theory of localized perturbations.[5,6] The first calculations[7–9] of the local-mode frequency treated the H^- ion in the mass-defect approximation. Later calculations[10–12] showed that force-constant changes must also be considered in order to explain both the local-mode frequency and the structure in the sidebands. In all of these calculations the force-constant changes were treated as adjustable parameters. However, good agreement with both the ultraviolet absorption and the infrared (ir) local-mode frequency has been obtained from first-principles quantum-mechanical calculations of the electronic structure of the U center.[13] A substitutional H^- ion in an alkali halide is particularly well suited for this type of calculation because it has relatively simple electronic structure and the same charge as that of the replaced ion, so that problems associated with electronic polarization and lattice relaxation are not insurmountable.

The primary purpose of the work described in this paper was to investigate the extent to which force constants calculated from first principles can explain the infrared properties of the U center. We have also studied the applicability of a Brillouin-zone integration technique described recently[14] to the numerical calculation of phonon Green's functions, and we shall comment briefly on this. For these purposes we have calculated the structure in the sidebands of the H^- local-mode frequency and the in-band absorption in the far-ir region. It should be clearly understood in advance that our calculations do not improve on the already excellent fit achieved in the most recent parametrized calculations,[15] although they do suggest some features not observed in previous experimental or theoretical work. One interesting by-product of

the calculations is the set of Born–Mayer parameters for the H^- ion which we have derived from quantum-mechanical calculations.

The paper is organized into six sections. In Sec. II we briefly describe the basic theoretical expressions with which we will be working. In Sec. III we describe the defect space, force-constant changes, and Green's functions. In Sec. V we treat the calculation of force constants and force-constant changes in detail. In Sec. V we discuss several aspects of our numerical calculations and give our results. Section VI contains a discussion of the work.

II. INFRARED ABSORPTION IN CRYSTALS CONTAINING POINT DEFECTS

The first-order resonance absorption of infrared radiation by lattice vibrations in a polar diatomic cubic crystal leads to a single absorption band at the reststrahl frequency. When an impurity is introduced, the translational invariance of the host lattice is destroyed, the so-called $q=0$ selection rule no longer holds, and absorption can occur throughout the entire range of phonon frequencies of the perturbed crystal. The absorption may indicate the occurrence of in-band resonances and true local modes both above the continuum and in the gap (if one exists) between the acoustical and optical regions. The absorption band due to a local mode may exhibit sidebands produced by the anharmonic interaction between the impurity and the host crystal. The general theory of these effects is now well understood and need not be described here since it has already been extensively applied to the U center in alkali halides. However, a few equations are needed in order to describe our own calculations, and for these we rely heavily on the work of Timusk, Klein, and co-workers, which has been discussed in a review article by Klein[16] and more recently in Ref. 15.

Timusk and Klein[11] have derived an expression for the absorption coefficient in the one-phonon sideband region of the U-center local mode. They point out that the lowest-order anharmonic interaction which will produce the sidebands gives a contribution to the Hamiltonian of the form

$$H_{\rm int} = \tfrac{1}{2} BQ^2X \,. \tag{1}$$

Q is the local-mode dynamical coordinate of T_{1u} symmetry and X is a configuration coordinate, which must have even parity. Because of the extremely light mass of the H^- ion, it is sufficient to limit Q to any one of the Cartesian displacements of that ion. Also, since the anharmonic coupling occurs almost entirely through the short-range forces, it is a good approximation to include only 1nn (first-nearest-neighbor) ions in the coordinate X. The exact form of X will be given later. B in Eq. (1) is the anharmonic-coupling coefficient, whose form need not concern us at the present level of approximation since it will be absorbed in an over-all normalization factor.

The expression obtained by Timusk and Klein for the sideband on the high-frequency side of the main band can be written as

$$I^+(\omega) = (hB^2/4\pi M^2\omega^2\Omega^2)\,\mathrm{Im}\langle X|\, G(\omega^2+i0^+)\,|X\rangle \,. \tag{2}$$

M is the mass of the hydrogen atom and Ω is the local-mode frequency with respect to which ω is given. The notation indicates that the limit of the imaginary part of the perturbed Green's function is to be taken as $\omega^2+i\epsilon$ approaches the real axis from above. G can be expressed in terms of the unperturbed Green's function G^0 as

$$G = (1+G^0\Delta)^{-1}G^0 \,. \tag{3}$$

Δ is the change in the dynamical matrix resulting from the introduction of the impurity; its form will be considered in more detail in Sec. III.

Klein[16] has derived the following expression for the infrared-absorption coefficient of an insulator containing point defects:

$$\alpha(\omega) = K(\omega)\,\mathrm{Im}\langle k_{\rm TO}, 0|\, t(\omega^2 - i0^+)\,|k_{\rm TO}, 0\rangle \,, \tag{4}$$

with

$$K(\omega) \propto \omega/n(\omega)\,(\omega_0^2-\omega^2)^2 \,. \tag{5}$$

$n(\omega)$ is the real part of the complex refractive index, which we have taken as

$$n^2(\omega) = \epsilon_\infty + (\epsilon_0-\epsilon_\infty)\,(1-\omega^2/\omega_0^2)^{-1} \,. \tag{6}$$

ϵ_0 and ϵ_∞ are the static and high-frequency dielectric constants, respectively. ω_0 is the frequency of the transverse-optical mode at $q=0$ and $|k_{\rm TO}, 0\rangle$ denotes the corresponding eigenvector. The t matrix for an isolated impurity is related to the unperturbed Green's function by

$$t = \Delta(1+G^0\Delta)^{-1} \,. \tag{7}$$

The calculation of the matrix elements of G in Eq. (3) and t in Eq. (7) is feasible because $(1+G^0\Delta)$ need be inverted only within the subspace for which Δ has nonvanishing matrix elements. This "defect space" will consist of the Cartesian displacements of the neighboring ions, and the matrix elements of G^0 in this representation must be found.

III. DEFECT SPACE, FORCE-CONSTANT CHANGES, AND GREEN'S FUNCTIONS

A. Defect Space

Following the work in Ref. 15, we have employed a "relaxation model" for the effect of the impurity on the host crystal. In this model it is assumed that the introduction of the defect produces an A_{1g} relaxation of the 1nn ions as well as a change in

TABLE I. Indexing of the defect ion and its first and fourth neighbors. The index ν is given in the body of the table.

n/site	000	100	010	001	$\bar{1}00$	$0\bar{1}0$	$00\bar{1}$
0	0	...	...	...	...	...	...
1	...	1	2	3	4	5	6
2	...	7	8	9	10	11	12

force constants between those ions and the defect site. In an A_{1g} relaxation, the six 1nn ions move inward or outward along the [100] directions. These displacements need not be more than a few percent of the nearest-neighbor distance to significantly alter the force constants between the first and fourth neighbors of the defect. In our calculations, then, the defect space consists of the Cartesian displacements of the defect ion, the six 1nn ions, and the six 4nn ions. The defect subspace therefore has maximum dimension of 39, but group-theoretical results can be used to greatly simplify the calculations.

The local-mode and far-ir absorption involve only those linear combinations of defect-space displacements which transform according to the $T_{1\mu}$ irreducible representation of the octadedral group, whereas the sidebands involve A_{1g}, E_g, and T_{2g}. We will refer to the various normalized combinations of Cartesian displacements as "symmetrized coordinates" and denote them by $Q_n(\Gamma_p)$; Γ gives the irreducible representation, n is an index which refers to the shells of equivalent ions involved in a particular Q, and p labels the orthogonal components which can be constructed for each n and Γ. We set $n=0$ for the defect site, $n=1$ for first-nearest neighbors, and $n=2$ for fourth neighbors. To simplify the notation, we assign an index ν to each ion in the defect space as shown in Table I.

The symmetrized coordinates of the defect space can now be written in terms of the small displacements from equilibrium. Generally we will denote these by $u_{i\nu}$, but for simplicity we will represent the Q's here by their subscripts i and ν, e.g., $u_{x0} \rightarrow x0$:

$$Q_0(T_{1u,1}) = x0\,, \tag{8a}$$

$$Q_0(T_{1u,2}) = y0\,, \tag{8b}$$

$$Q_0(T_{1u,3}) = z0\,; \tag{8c}$$

$$Q_1(A_{1g}) = (1/\sqrt{6})\,(x1 - x4 + y2 - y5 + z3 - z6)\,, \tag{9a}$$

$$Q_1(E_{g,1}) = (1/2\sqrt{3})\,[2(x1 - x4) - y2 + y5 - z3 + z6]\,, \tag{9b}$$

$$Q_1(E_{g,2}) = \tfrac{1}{2}\,(y2 - y5 - z3 + z6)\,; \tag{9c}$$

$$Q_1(T_{2g,1}) = \tfrac{1}{2}\,(z2 + y3 - z5 - y6)\,, \tag{10a}$$

$$Q_1(T_{2g,2}) = \tfrac{1}{2}\,(z1 + x3 - z4 - x6)\,, \tag{10b}$$

$$Q_1(T_{2g,3}) = \tfrac{1}{2}\,(y1 + x2 - y4 - x5)\,; \tag{10c}$$

$$Q_1(T_{1u,1}) = (x1 + x4)/\sqrt{2}\,, \tag{11a}$$

$$Q_1(T_{1u,2}) = (y2 + y5)/\sqrt{2}\,, \tag{11b}$$

$$Q_1(T_{1u,3}) = (z3 + z6)/\sqrt{2}\,. \tag{11c}$$

For each $Q_1(\Gamma_p)$ there is an exactly analogous $Q_2(T_p)$ involving the displacements of the ions in the fourth shell, but it is not necessary to write them out since they are obtained simply by the appropriate change in the subscript ν.

The configuration coordinate X appearing in Eqs. (1) and (2) can now be defined in terms of the Q's. When the H^- ion is vibrating in the x direction, Timusk and Klein assumed that

$$X = (x1 - x4)/\sqrt{2}\,, \tag{12}$$

which implies that the anharmonic coupling with the lattice takes place through the parallel force constants between H^- and the 1nn ions. Intuitively this is a good approximation and subsequent experience has supported its validity. From Eq. (12), X can be written in terms of the Q's as

$$X = [Q_1(A_{1g}) + (\sqrt{2})\,Q_1(E_{g,1})]/\sqrt{3}\,. \tag{13}$$

The coupling to T_{2g} modes is quite small and will be neglected entirely here.

B. Force-Constant Changes

The potential energy of the crystal can be expanded in terms of small displacements of the ions from their equilibrium positions in the usual way, i.e.,

$$U = U_0 + \frac{1}{2}\sum_{i\mu}\sum_{j\nu} K_{i\mu,j\nu}\,u^*_{i\mu}\,u_{j\nu}\,. \tag{14}$$

As before, μ and ν are site indices, i and j run over the Cartesian coordinates, and

$$K_{i\mu,j\nu} \equiv \left(\frac{\partial^2 U}{\partial u_{i\mu}\,\partial u_{j\nu}}\right)_0\,. \tag{15}$$

The potential energy can also be expanded in terms of a complete set of symmetry coordinates of the type defined above for the defect space. Thus,

$$U = U_0 + \frac{1}{2}\sum_{nm}\sum_{\Gamma p} \mathcal{K}_{nm}(\Gamma p)\,Q_n(\Gamma p)\,Q_m(\Gamma p)\,, \tag{16}$$

with

$$\mathcal{K}_{nm}(\Gamma p) \equiv \left(\frac{\partial^2 U}{\partial Q_n(\Gamma p)\,\partial Q_m(\Gamma p)}\right)_0\,. \tag{17}$$

n and m run over all the shells of equivalent ions in the crystal, Γ runs over the irreducible representations of the point group, and p again labels the orthogonal components of each Γ. The contribution to a defect matrix element from the force-constant changes can now be defined by

$$\Delta_{nm}(\Gamma p) = \mathcal{K}_{nm}(\Gamma p) - \mathcal{K}^0_{nm}(\Gamma p) , \tag{18}$$

where the superscript 0 denotes the force constants of the perfect crystal and the $\mathcal{K}_{nm}(\Gamma p)$ are the force constants when the substitutional impurity is present.

The advantage of working the Q representation is that the force constants are diagonal with respect to Γ and p. For a defect space consisting of the displacements of the impurity and the first few shells of neighboring ions, it is quite feasible with the aid of a computer to evaluate the second derivatives in Eq. (16) directly. Such an approach will show clearly that the force-constant changes for the various symmetry modes are by no means the same. Although this may be an important consideration for some types of impurities, we do not believe it is for the U center. Therefore, in order to make more direct comparisons with quantities appearing in the shell model, we will relate the force constants $\mathcal{K}$ and K by using the transformation

$$u_{i\mu} = \sum_n \sum_{\Gamma p} \langle u_{i\mu} | Q_n(\Gamma p)\rangle \, Q_n(\Gamma p) . \tag{19}$$

We find that

$$\mathcal{K}_{nm}(\Gamma p) = \sum_{i\mu} \sum_{j\nu} \langle Q_n(\Gamma p) | u_{i\mu}\rangle K_{i\mu,j\nu} \langle u_{j\nu} | Q_m(\Gamma p)\rangle . \tag{20}$$

This equation makes it very simple to generate the $\mathcal{K}_{nm}(\Gamma p)$ from the force constants between individual ions (the $K_{i\mu,j\nu}$) when only repulsive interactions are considered.

C. Green's Functions

We saw in Sec. II that both the anharmonic sidebands and the far-ir absorption directly involve various symmetry projections of the Green's function of the crystal containing the impurities and these, in turn, involve the Green's functions of the perfect crystal, i.e., G^0 of Eq. (3). A representation of G^0 in terms of the symmetry coordinates $Q_n(\Gamma p)$ is easily found. First we note that G^0, like the dynamical matrix itself, is diagonal with respect to Γ and p, and so we can write

$$\begin{aligned} G^0_{nm}(\omega^2, \Gamma p) &= \langle Q_n(\Gamma p) | G^0 | Q_m(\Gamma p)\rangle \\ &= \sum_{\vec{q}j} \sum_{\vec{q}'j'} \langle Q_n(\Gamma p) | v(\vec{q}j)\rangle \langle v(\vec{q}j) | G^0 | v(\vec{q}'j')\rangle \langle v(\vec{q}'j') | Q_m(\Gamma p)\rangle \\ &= \sum_{\vec{q}j} \langle Q_n(\Gamma p) | v(\vec{q}j)\rangle [\omega^2 - \omega^2(\vec{q}j)]^{-1} \langle v(\vec{q}j) | Q_m(\Gamma p)\rangle . \end{aligned} \tag{21}$$

$v(\vec{q}j)$ is the phonon eigenvector of the perfect crystal with wave number $\vec{q}$ and branch index j. We have used the closure relationship and the fact that G^0 is diagonal with respect to the phonons of the perfect crystal with eigenvalue $[\omega^2 - \omega^2(\vec{q}j)]^{-1}$. The v's are given by

$$v(\vec{q}j) = N^{-1/2} \sum_{\alpha\kappa l} (M_\kappa)^{-1/2} e_\alpha(\kappa; \vec{q}j) e^{i\vec{q}\cdot\vec{R}(l)} , \tag{22}$$

in which $e_\alpha(\kappa; \vec{q}j)$ is the αth Cartesian component of the polarization vector of the κth type of ion in the $\vec{q}j$th normal mode. $\vec{R}(l)$ is a lattice vector.

We now add a small imaginary part ϵ to the frequency and find the limit as ϵ approaches zero. Denoting this limit as before by 0^+ and using the well-known relationship

$$\lim(x + i\epsilon)^{-1} = PP(x^{-1}) - i\pi\delta(x) \quad \text{as} \quad \epsilon \to +0 , \tag{23}$$

we find for the imaginary part of the matrix elements of G^0

$$\begin{aligned} \mathrm{Im}G^0_{nm}(\omega^2, \Gamma p) = \pi \sum_{\vec{q}j} \langle Q_n(\Gamma p) | v(\vec{q}j)\rangle \\ \times \langle v(\vec{q}j) | Q_m(\Gamma p)\rangle \, \delta(\omega^2 - \omega^2(\vec{q}j)) , \end{aligned} \tag{24a}$$

$$\begin{aligned} \mathrm{Im}G^0_{nm}(\omega, \Gamma p) = \frac{\pi}{2\omega} \sum_{\vec{q}j} \langle Q_n(\Gamma p) | v(\vec{q}j)\rangle \\ \times \langle v(\vec{q}j) | Q_m(\Gamma p)\rangle \, \delta(\omega - \omega(\vec{q}j)) . \end{aligned} \tag{24b}$$

Once the imaginary parts have been found by numerical techniques, the real parts can be found by using the Kramers–Kronig dispersion relations in conjunction with a scheme for evaluating the principal part of the integral. This has become a fairly straightforward calculation by now and we need not go into it here since again we have followed Timusk and Klein closely. The numerical calculation of the imaginary parts is of more interest and we shall return to it in Sec. V. We note here a sum rule or normalization condition for $\mathrm{Im}G^0$ which is indispensable in the numerical work. We integrate Eq. (24b) over ω and carry out the summation over $\vec{q}j$ to find

$$\pi^{-1} \int \mathrm{Im}G^0_{nm}(\omega, \Gamma p) \, 2\omega \, d\omega = \delta_{nm} . \tag{25}$$

IV. CALCULATION OF FORCE-CONSTANT CHANGES

Quantum-mechanical calculations of the electronic structure of the H^- ion in various host alkali halide crystals have been carried out by Wood and Öpik[13] and Wood and Gilbert.[13] These calculations give the energy of the H^- ion as a function of the displacements of the six 1nn ions and should therefore provide force constants for A_{1g} and E_g displacements. The calculations also give the energy of the H^- ion when it is displaced while all of the other ions are held fixed in their equilibrium positions. The H^- ion is polarized in this type of displacement and a force constant for the T_{1u} local mode can be extracted and used in the far-ir calculations. We will first discuss the various contributions to the energy of the H^- ion and relate them to quantities appearing in classical ionic-crystal theory when possible.

A. Quantum-Mechanical Treatment of H^- Ion

The energy of the substitutional H^- ion in the crystal is composed of several terms all of which depend on the positions of the 1nn ions. For comparison with the classical Born–Mayer treatment of ionic crystals, we break the energy up into Madelung and repulsive terms, i.e.,

$$E(R) = E_M(R) + E_r(R) \ . \tag{26}$$

The dependence of the Madelung term on the nearest-neighbor distance R can be made explicit by writing

$$E_M(R) = -\alpha_M/R_0 + 6Z_H Z_A(R^{-1} - R_0^{-1}) \ . \tag{27}$$

α_M is the Madelung constant, R_0 the 1nn distance in the perfect crystal, and Z_H and Z_A the effective charges of the H^- and alkali ions, respectively. The calculations in Ref. 13 do not treat E_M as a separate term, and in subtracting it from $E(R)$ in order to find $E_r(R)$ we have assumed that $Z_H = -1$ and $Z_A = +1$. As noted below, an argument can be made for taking $|Z_H|$ somewhat less than unity, which resembles a result in shell-model calculations. We prefer, however, to include the effect in the repulsive energy.

The repulsive energy is quite complicated and so we shall break it up as follows:

$$E_r(R) = E_s(R) + \Delta E_M(R) + E_{ex}(R) + E_{co}(R) + E_{ov}(R) \ . \tag{28}$$

E_s might be referred to as the self-energy of the H^- ion, since it contains those terms such as electronic kinetic energy and electron-nuclear and electron-electron interaction energies which would contribute to the total energy of an H^- ion in free space. It even contains a substantial amount of the correlation energy of the H^- ion, since correlated wave functions of the Hylleraas type were used in the quantum-mechanical calculations. The H^- ion is not quite stable in free space, whereas, in its ground state in the crystal, it is stabilized and confined to the negative-ion vacancy, primarily by the Madelung potential. If E_s is expanded about the equilibrium value of R, the largest contribution by far comes from the constant term, but higher-order terms do contribute and can alter the force constants.

The term ΔE_M comes about because the H^- ion is not a point charge as was assumed when writing Eq. (27). Since the tail of the H^- wave function extends beyond some of the shells of ions, these ions do not see a unit point charge at the impurity site. Calculations indicate that approximately 95% of the charge of the H^- ion is within the 1nn distance. As mentioned above, it would be possible to account for ΔE_M approximately by introducing an effective charge Z_H into Eq. (27).

The terms E_{ex} and E_{co} are the exchange and Coulomb interaction energies between the H^- ion and the six 1nn ions. E_{ex} is attractive and thus reduces the total repulsive energy. Because the ions of the host crystal are treated as unit point charges when the Madelung energy is calculated, the quantity E_{co} is really a "penetration energy" and is, in fact, also attractive. It arises because the electrons of the H^- ion are able to penetrate the extended charge distributions of the neighboring ions, so that the electrons on these ions are not able to fully screen the nuclear charge.

E_{ov} is the overlap repulsive energy arising from the orthogonalization of the H^- wave function to the orbitals on the neighboring ions. It yields the largest single contribution to the repulsive force constants but it is erroneous to think of it as the *only* term which contributes, as seems to be implied in many discussions of lattice dynamics. We note also that, primarily because of the orthogonalization condition, it is not entirely possible to break the energy up into a sum of two-body interactions as is generally done. Nevertheless, the error made in assuming that one can do so is probably not great for alkali halide crystals and we will utilize this approximation in the present calculations.

When the H^- ion is substituted into the crystal, the neighboring ions will move to new equilibrium positions. This produces a change in the energy of the host crystal which we denote by ΔE_{cr}. That part of the total electronic and ionic energy which will be important for determining the potential energy at ionic displacements can now be written as

$$U(R) = E(R) + \Delta E_{cr}(R) \ . \tag{29}$$

In Ref. 13, ΔE_{cr} was calculated as a function of 1nn displacements only. In the present calculations, the change in repulsive force constants between first and fourth neighbors plays a role, and it would

seem advisable to also consider the displacement of 4nn ions. We have studied the effects of 4nn displacements to a limited extent and have concluded that they are rather small for the U center in its ground state. In view of the present over-all accuracy of our calculations it seems unnecessary to include them here. The second- and third-neighbor displacements, besides having little effect on the force constants, are expected to be very small indeed.

We conclude this subsection by noting that in a T_{1u} mode in which only the H^- ion is displaced there is a substantial contribution to the energy which comes about because the H^- ion can be easily distorted or polarized. In the first-principles calculations this polarization energy is not treated as a separate term, and we will not attempt to extract it here. Its effect on the T_{1u} force constants is large, and will be discussed below.

B. Calculation of H^--K^+ Force Constants

Repulsive force constants can be determined from the quantum-mechanical calculations outlined above. We assume that the change in potential energy [Eq. (29)] due to an A_{1g} displacement of the 1nn ions can be expanded in terms of the coordinate $Q_1(A_{1g})$ as

$$\Delta U_{11}(A_{1g}) = \tfrac{1}{2}\mathcal{K}_{11}(A_{1g})\,Q_1^2(A_{1g})\,. \tag{30}$$

In fact, this is a good approximation, with fourth-order terms in Q_1 contributing very little. Correspondingly, we also write

$$\Delta U_{11}^r(A_{1g}) = C_1\,Q_1(A_{1g}) + \tfrac{1}{2}\mathcal{K}_{11}^r(A_{1g})\,Q_1^2(A_{1g})\,, \tag{31}$$

where $\mathcal{K}_{11}^r$ is the repulsive force constant for an A_{1g} displacement of the 1nn ions. Because the repulsive interactions are short ranged, the K^+-K^+ interactions in KCl, KBr, and KI are negligible. In such cases it is easily shown that the repulsive force constants for 1nn motion are the same in the A_{1g} and E_g modes. This is not true for the contributions from ΔE_{cr} and E_M. Thus there is no reason why the total force constants for the different modes should be the same, as has been assumed in the past. We have found, however, that because of the small 1nn displacements for the U center, the force-constant *changes* arising from ΔE_{cr} and E_M are small compared with those arising from E_r. In fact, the only really important changes are the 1nn defect and the 1nn-4nn repulsive interactions. Because of this and the form of the Q's, we can write, e.g.,

$$\mathcal{K}_{11}^r(A_{1g}) = K_1 + K_2\,. \tag{32}$$

K_1 and K_2 are, respectively, the parallel force constants between a single 1nn ion and the H^- ion and between nearest neighbors in the first and fourth shells. K_1 can be determined from the quantum-mechanical calculations since E_r [Eq. (28)] is given in the neighborhood of the equilibrium positions of the ions. In Table II, we show K_1 as a function of the 1nn displacements in order to indicate the sensitivity of the repulsive force constants to the positions of the 1nn ions. One of the problems in attempting to calculate force-constant changes rather than treating them as parameters is the difficulty in determining the positions of the ions accurately when the impurity is present. Once these positions have been established, however, K_2 can be easily obtained from Born–Mayer potentials of the perfect crystal.

TABLE II. Repulsive force constant K_1 in Eq. (32) as a function of the 1nn displacements. δ is given as a percentage of the nearest-neighbor distance and a minus sign indicates an inward displacement. K_1 is in dyn/cm.

δ	KCl	KBr	KI
0	14 100	9 830	6110
−1	15 150	10 560	6530
−2	16 220	11 320	7050
−3	17 330	12 130	7540
−4	18 470	13 040	8110

It is both interesting and useful to cast our H^--K^+ repulsive potential energy into the well-known exponential form introduced by Born and Mayer. To facilitate this, we change our notation somewhat and approximate E_r by

$$E_r(Z) = C + 6R(z)\,, \tag{33}$$

with

$$R(z) = A\,e^{-(z-\bar{z})/\rho}\,. \tag{34}$$

Here, z is the distance between the H^- and 1nn K^+ ions in an A_{1g} mode. C, A, and ρ are parameters to be determined from the quantum-mechanical calculations. Both C and A are functions of the reference position $\bar{z}$, but we will not explicitly indicate this in the notation. The constant C appears because the self-energy term discussed above is quite large even when $\bar{z}$ is near the perfect-crystal equilibrium value. Denoting the first and second derivatives of $R(z)$ with respect to z by a prime and double prime, respectively, we have

$$\rho = -R'(\bar{z})/R''(\bar{z})\,, \tag{35}$$

in which the derivatives are to be evaluated numerically at $z=\bar{z}$ from the quantum-mechanical calculations. Once ρ is known, A can be determined from the force constants of Table II, since from Eq. (34)

$$K_1(\bar{z}) = R''(\bar{z}) = A/\rho^2\,. \tag{36}$$

With ρ and A known, C can easily be found, although it is not necessary for our purposes. Table III

TABLE III. Born–Mayer (BM) parameters for the H^- ion. $\bar{z}$ is the H^--K^+ distance at which the parameters were evaluated. In KCl and KBr it is R_0 and in KI it corresponds to a 1% inward displacement. The last three columns indicate the quality of fit achieved by the Born–Mayer form at 2% inward displacements from $\bar{z}$. QM stands for "quantum mechanical."

	$\bar{z}$ (Å)	C (eV)	A (eV)	ρ (Å)	δ	Energy comparison (in eV) QM	BM
KCl	3.14	−13.3720	0.1998	0.476	−2	−12.0045	−12.0041
KBr	3.30	−13.4525	0.1511	0.496	−2	−12.4174	−12.4170
KI	3.495	−13.5705	0.1157	0.533	−3	−12.7787	−12.7779

shows the values of C, A, ρ, and $\bar{z}$ for the three crystals considered here. Note that $\bar{z}$ need not be the equilibrium value of z, although it should be fairly close to it in order to increase the accuracy of Eq. (33).

For the T_{1u} mode, we have taken the H^--K^+ force constants directly from Ref. 13. We chose those values which include polarization of the H^- ion but not 2nn interactions. The polarization effect decreases the T_{1u} force constant by approximately 40% in KCl and cannot be ignored. As we shall see, determining the T_{1u} force constants for the perfect crystal is not entirely straightforward.

C. Force Constants for Perfect Crystal

In order to calculate the change in force constants when the impurity is introduced, we must know the force constants of the perfect crystal. Values can be obtained from shell-model fits to phonon-dispersion curves as long as the ions are in their perfect-crystal positions, but these values do not provide estimates of the changes due to the displacement of the ions. These can be found if a reasonably accurate Born–Mayer potential for the repulsive interaction is known. We believe that the work of Tosi and Fumi[17] yields the most reliable potentials, and since they were used in calculating the relaxation around the H^- ion, it seems reasonable to use them here for the perfect crystal.

In the perfect crystal, the repulsive force constant for the alkali ion at the 100 site participating in either an A_{1g} or an E_g displacement about a halide ion at the 000 site is

$$\mathfrak{K}_{11}^{r_1 0} = 2K_1^0 + 4K_\perp^0 , \tag{37}$$

in which

$$K_1^0 = R''(z_0) , \quad K_\perp^0 = z_0^{-1} R'(z_0) . \tag{38}$$

$K_\perp^0$ is the perpendicular force constant coupling the K^+ ion in the 100 position to the halide ions in the 110, 101, $1\bar{1}0$, and $10\bar{1}$ positions; $K_\perp^0$ couples the 100 ion to the 000 ion and the 200 ion. In alkali halide crystals, $K_\perp^0$ is negative and usually of the order of 10% of K_1^0. Unless the introduction of the H^- ion results in a quite substantial displacement of the 100 ion from its perfect-crystal position, the change in $K_\perp^0$ will be negligibly small compared with the change in K_1^0. However, even small displacements can result in large changes in K_1^0.

Corresponding to Eq. (34) for the defect, we take for the perfect crystal

$$\mathfrak{R}(z) = \mathfrak{a} e^{-(z-z_0)/\rho_0} , \tag{39}$$

and find that

$$K_1^0 = \mathfrak{a}/\rho_0^2 , \qquad K_\perp^0 = -\mathfrak{a}/z_0\rho_0 . \tag{40}$$

Tosi and Fumi have given two sets of parameters which when used in Eq. (40) give very nearly the same results for the force constants. We have calculated K_1^0 and $K_\perp^0$ with both sets, and in Table IV we compare them with the corresponding values found from shell-model fits to phonon-dispersion curves. We have shown the estimated uncertainties in the shell-model K_1^0 and comparable ranges exist for the Tosi–Fumi values. The agreement between the three sets of values is remarkably good and suggests that the Tosi–Fumi values might be of use in shell-model calculations. The agreement between the $K_\perp^0$ values is also quite good, but for reasons we need not consider here they are not exactly comparable in principle. We also note that Tosi and Fumi determined the parameters in their potentials from room-temperature data, whereas the phonons in the shell-model work were measured at approximately 100 °K.

We believe the methods outlined in the foregoing

TABLE IV. Comparison of perfect-crystal force constants. The Tosi–Fumi values calculated from Born–Mayer potentials of Ref. 17. The shell-model parameters were taken from the references indicated.

	Tosi–Fumi (first set) K_1^0	$K_\perp$	Shell model K_1^0	$K_\perp$	Tosi–Fumi (second set) K_1^0	$K_\perp$
KCl	22 651	−2431	23 042 ± 1008[a]	−2091	24 042	−2481
KBr	20 987	−2130	21 495 ± 441[b]	−1945	21 016	−2121
KI	17 089	−1719	18 119 ± 676[c]	−1474	17 662	−1731

[a] J. R. D. Copley, R. W. MacPherson, and T. Timusk, Phys. Rev. 182, 965 (1969); Phys. Rev. B 1, 4193 (E) (1970).

[b] R. A. Cowley, W. Cochran, B. N. Brockhouse, and A. D. B. Woods, Phys. Rev. 131, 1030 (1963).

[c] G. Dolling, R. A. Cowley, C. Schittenhelm, and I. M. Thorson, Phys. Rev. 147, 577 (1966).

TABLE V. Force-constant changes for the A_{1g} and E_g modes calculated as indicated in the text. All force constants are in dyn/cm.

	KCl	KBr	KI
δ	−0.7	−1.5	−2.3
ρ_0	0.324	0.333	0.346
K_1	14 800	11 000	7 250
ΔK_1	−9 240	−10 020	−10 410
ΔK_2	−1 580	−2 900	−3 700

discussion give the A_{1g} and E_g repulsive force constants of the perfect crystal with an accuracy consistent with that of the U-center calculations. The methods fail for the T_{1u} mode because the parameters in the potentials do not account for the electronic and displacement polarizabilities of the ions. Although it might be possible to extract information about these quantities from shell-model parameters, we have found it more satisfactory to employ a simple modification of a procedure described by Klein in Ref. 16. In this approach all ions except the one at the 000 site are held fixed in their perfect-crystal positions. The force constant coupling this central-site ion to the lattice is then varied until an instability occurs. This instability is indicated by a resonance at zero frequency, and the corresponding force-constant change is just the negative of an "effective force constant" K_{eff} for that ion. The equation for determining it in this manner can be obtained from $\det|1+G^0\Delta|=0$ and is given by

$$K_{\text{eff}} = M_-/2\,\text{Re}G^0_{00}(0, T_{1u}) , \tag{41}$$

in which M_- is the mass of the halide ion and $G^0_{00}(0, T_{1u})$ is the zero-frequency limit of the matrix element of the Green's function between one of the coordinates defined in Eqs. (8a)–(8c). Our method of determining K_{eff} differs slightly from that described by Klein in that he uses the matrix element of G^0 in a configuration which allows both the 1nn and central-site ions to move. We feel, and our results seem to bear it out, that it is better to let only the central ion move, since the force constants for the H^- ion are determined under this same condition.

D. Force-Constant Changes

We finally have all the information necessary to calculate force-constant *changes*. Table V gives the data for the force-constant changes used in the sideband calculation, i.e., for A_{1g} and E_g modes. δ is the percentage inward displacement of the 1nn ions in terms of the nearest-neighbor distance. K_1^0 is taken from column 3 of Table IV, K_1 is extracted from Table II by graphical interpolation, and $\Delta K_1 = K_1 - K_1^0$. ΔK_2 is computed from Eqs. (39) and (40), again using the second set of data from Tosi and Fumi for the perfect crystal and the values of δ in the top row. We also show the "hardness" parameter ρ for comparison with the values in Table III for the H^--K^+ interaction. A small value of ρ indicates a "hard" ion and it can be seen that the H^- ion is relatively soft compared with the halides it replaces.

Table VI gives the T_{1u} force-constant changes involved in the infrared absorption. K_{eff} was calculated from Eq. (41). K_U was calculated from the frequencies given in column 3 of Table II in Ref. 13. These frequencies included the effects of H^- polarization but not the interactions of the H^- ion with its second-nearest neighbors. Note that both K_{eff} and K_U are one-half of the total force constant coupling the central site to the rest of the crystal. ΔK_2 involves only the ions of the perfect crystal and has been assumed to be the same in all modes.

With the force-constant changes calculated it is straightforward to construct the defect matrix, and we can now proceed to the calculation of the absorption coefficient via Eqs. (2) and (4).

V. NUMERICAL TECHNIQUES AND RESULTS

A few details of the numerical techniques used in the calculations may be of interest to some readers. Two methods were used to evaluate the imaginary part of the Green's functions in Eq. (24b). For most of the calculations a combined linear- and quadratic-interpolation (CLQ) scheme described in a recent paper by Cooke and Wood[14] was utilized. The final calculations were then carried out within the framework of the well-known Gilat–Raubenheimer (GR) method[18] which employs linear interpolation and extrapolation only. The rationale for this is that our experience with the two methods, in the form we are using them, shows that the CLQ scheme is considerably faster than the GR scheme, but that the latter is probably more accurate if sufficiently small meshes are used. The reasons for these relative merits are rather subtle and we will not discuss them here since they may change with further developments.

In most of the calculations with the CLQ scheme the eigenfrequencies, eigenvectors, and overlap integrals $\langle v(\vec{q}j)|Q(\Gamma p)\rangle$ of Eq. (24b) were evaluated

TABLE VI. Force-constant changes for the T_{1u} mode calculated as indicated in the text. Here $\Delta K_1 = K_U - K_{\text{eff}}$ and the force constants are in dyn/cm. M_- is the mass of the negative ion in amu.

	M_-	K_{eff}	K_U	ΔK_1	ΔK_2
KCl	35.457	17 960	6860	−11 590	−1580
KBr	79.909	15 040	5350	−9 690	−2900
KI	126.904	12 560	3700	−8 860	−3700

from shell-model results at 916 points in the irreducible sector of the Brillouin zone (BZ). These first-principles values were then used in a quadratic interpolation over a regular mesh formed by dividing the Γ-to-X direction in the BZ into ten equal intervals. Twenty-seven first-principles points are used in each of these cells to determine by a least-squares fit the ten independent coefficients in the quadratic-interpolation formulas. After this step the products of the overlap integrals and the frequencies are given in analytic form throughout the entire BZ. Next a finer mesh is formed within the quadratic mesh. The products of overlap integrals are determined at the center of each of these fine mesh cells and assumed to have this value throughout the cell. The analytic integration introduced by Gilat and Raubenheimer is then used to determine $\mathrm{Im}G^0_{nm}$ from Eq. (24b). It is not necessary to hold the overlap integrals constant within the small cells, but we have such a fine mesh that it has proved to be quite an acceptable approximation. Once the imaginary parts of the Green's functions have been found, the real parts can be found straightforwardly via the Kramers–Kronig dispersion relations as already mentioned.

In practice, though not in principle, the BZ integration schemes we have used both represent the Green's functions by histograms. Generally speaking, we have tried to keep the histogram box width of the order of 0.02 THz. When calculating the perturbed Green's functions we have found it useful to employ complex arithmetic, matrix inversion, etc., directly in the machine and separate the real and imaginary parts at the end of the calculations. We have also found that the programs are so fast on the IBM 360/91 that the entire calculation including the generation of the first-principles eigenvectors, eigenvalues, and overlap integrals, the evaluation of the unperturbed Green's functions, the inversion of complex matrices, etc., can be carried through from the beginning each time. A typical run requires about $1\frac{1}{2}$ min to generate the Green's functions. After that the final results for a very large number of force-constant and mass changes can be generated with little additional computer time.

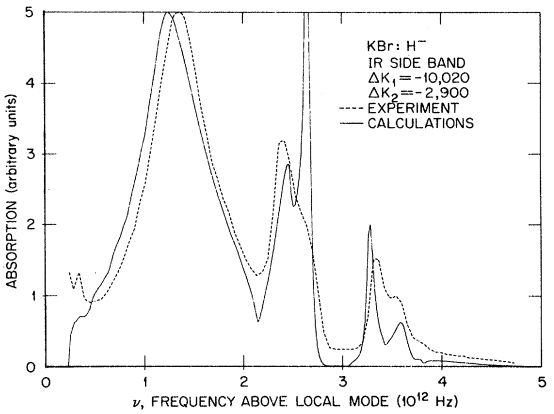

FIG. 2. Anharmonic sideband of the local-mode frequency of H^- ions in KBr.

The results of the infrared sideband calculations are shown in Figs. 1–4. The dashed curves were taken as best we could from the work in Ref. 15. All of the curves have been normalized to the broad low-frequency peak in order to avoid anharmonic effects associated with sharp narrow resonances. We have shown two curves for KI in order to illustrate the sensitivity of the calculations to small changes in the force constants. The region just above the local-mode reference frequency is subject to considerable uncertainties. For example, the origin of the structure below 1 THz in the experimental curve for KCl is not clear. On the other hand, the calculated curves also have uncertainties associated with them in this region because of poor

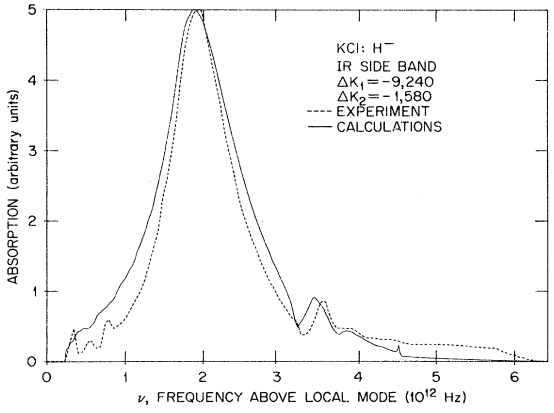

FIG. 1. Anharmonic sideband of the local-mode frequency of H^- ions in KCl.

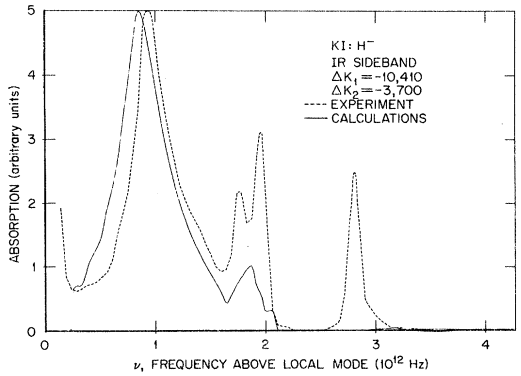

FIG. 3. Anharmonic sideband of the local-mode frequency of H^- ions in KI. The calculations give an E_g gap mode at ~ 2.2 THz and an A_{1g} gap mode at ~ 2.8 THz.

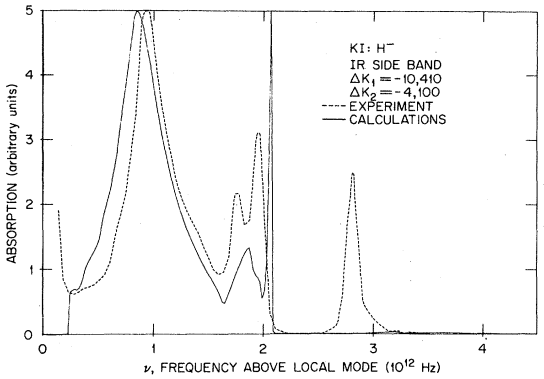

FIG. 4. Anharmonic sideband of the local-mode frequency of H^- in KI. The E_g mode has now moved just out of the gap to ~ 2.2 THz, whereas the A_{1g} mode remains in the gap. Note the small change in ΔK_2 to accomplish this.

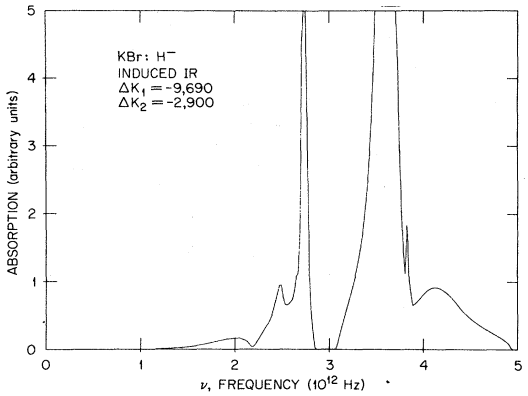

FIG. 6. Induced infrared absorption in KBr: H^-.

statistics in the histogram boxes at these low frequencies. The calculated curves could easily be smoothed, but since the experimental uncertainties would remain, we have cut all curves near the origin as a reminder that there are minor problems in this region.

Figures 5–7 show our results for the far-ir absorption. We have not given measured curves, because it seemed to us that the accuracy of the experimental work did not warrant a detailed comparison.

VI. DISCUSSION

The agreement between the calculated and experimental sidebands is generally quite impressive. Reasons for the disagreements that do exist, other than the obvious possibility that our model may not be exactly correct, are that (i) both the experimental and calculated unperturbed phonon frequencies may be in error by as much as 3 cm^{-1} (~ 0.1 THz) at some points in the BZ, (ii) the shell-model eigenvectors used in the overlap integrals may have substantial errors, (iii) the infrared measurements have an estimated accuracy of ± 1 cm^{-1}, and (iv) there may be numerical inaccuracies in our calculations in addition to those associated with the unperturbed phonons and the determination of force-constant changes. Some of these errors will undoubtedly tend to compensate one another, e.g., the least-squares fitting of shell model to measured frequencies. In fact, we had anticipated fairly good agreement with experiment, since our calculated values of ΔK_1 and ΔK_2 are fairly close to the parametrized values of MacPherson and Timusk. For $(-\Delta K_1, -\Delta K_2)$ in KCl, KBr, and KI these authors found (9095, 0), (8855, 4100), and (8945, 5150), respectively.

It would appear from the calculations on KI that rather small changes in the force constants can produce drastic changes in the sideband spectra, but these are more apparent than real. In the calculations of Fig. 3, a local mode of E_g symmetry lies just above the edge of the acoustical band at 2.1 THz, and in the calculations of Fig. 4 this mode has just moved into the band to produce the large

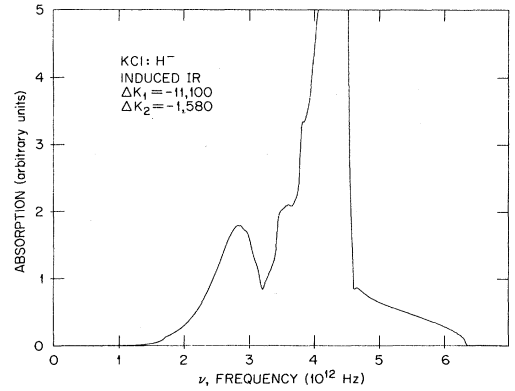

FIG. 5. Induced infrared absorption in KCl: H^-.

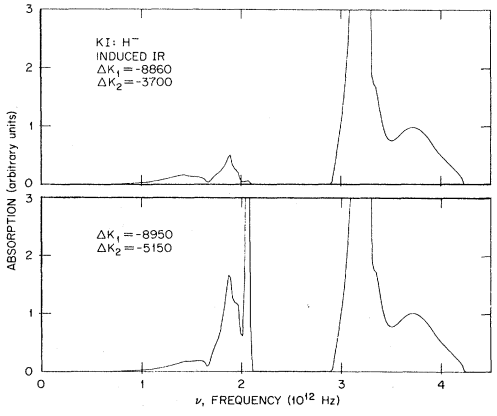

FIG. 7. Induced infrared absorption in KI: H^-.

resonance shown. Had we chosen to show the local mode on Fig. 3 and if we were able to calculate its anharmonic broadening, the structure on the two figures would be very much the same. The parametrized calculations in Ref. 15 give a somewhat better fit in the case of KI than we obtain. A comparison of their force-constant changes with ours indicates that our values of ΔK_2 are probably somewhat small. The most likely reason for this is an inaccurate determination of the relaxed positions of the 1nn ions. In contrast to the situation in KI, our calculations for KCl showed that fairly substantial changes in ΔK_2 hardly affected the spectrum. In fact, the choice of $\Delta K_2 = 0$, as in Ref. 15, gives agreement with experiment comparable to that in Fig. 1. This insensitivity to ΔK_2 undoubtedly stems from the lack of a true resonance in the KCl case. The small spike on the KCl curve at $\simeq 4.5$ THz is a remnant of the very sharp, intense spike in the unperturbed density of states at the same frequency.

The importance of anharmonic effects is indicated in the experimental results for KI. The peak at approximately 2.8 THz is due to a true local mode of A_{1g} symmetry whose broadening is most likely due primarily to anharmonic interactions with the perturbed band modes. It seems safe to assume that a somewhat comparable broadening can be expected for resonances which are sharp in the harmonic approximation. For this reason alone we would not expect to get very accurate agreement with the intensities and widths of some of the sharper features of the spectrum.

In a series of calculations on KBr in which ΔK_2 was changed in steps of 300 dyn/cm, the intensities in the two peaks between 2 and 3 THz could be shifted relative to each other and to the rest of the spectrum without greatly altering their frequencies. Some one or more of these results might be superior to that shown in Fig. 2, but in the light of the other inaccuracies in calculated and experimental values and the neglect of anharmonic interactions we feel that our calculated force constants are quite satisfactory.

On first inspection, the calculated far-ir spectra bear only a qualitative resemblance to the experimental results of MacPherson and Timusk as given in the third paper of Ref. 15. Closer examination shows that there are, in fact, quantitatively similar features in the calculated and measured curves and we shall concentrate our attention on these.

The measured absorption in KCl:H^- shows a broadband peaking at about 2.97 THz and a much narrower peak at 3.27 THz followed by the sharply rising absorption in the reststrahl region. Our calculated curve gives the broad peak very well, shows no trace of the 3.27-THz peak, and indicates a pronounced shoulder at 3.51 THz. In very recent work, Ward and Timusk[19] have measured the far-ir absorption for KCl and KBr containing many different impurities. In KCl their results can be summarized by saying that there is always a peak at about 3.27 THz, a sharp minimum at 3.30 THz, and a broad shoulder and sometimes an actual peak at about 3.51 THz. Ward and Timusk suggest that the 2.97-THz peak in the work of Ref. 15 is due to a resonance and that the 3.27-THz peak is the same one exhibited by all other impurities in KCl and is most likely due to a Van Hove singularity in the unperturbed density of states. We suspect that the work of MacPherson and Timusk may have simply missed the 3.51-THz shoulder in KCl:H^-. This would leave only the 3.2-THz peak unaccounted for by the calculations. Assuming the experimental results are correct, it seems to us that there are two likely explanations for the discrepancy: (a) The shell-model phonons and eigenvectors for KCl are not accurate enough in this region and (b) the two interpolation schemes we have used may encounter difficulties in regions where the eigenvectors and frequencies are changing rapidly. There is another interesting feature of the KCl calculations which does not appear in the experimental curves published thus far but which would probably show up with better resolution. This is the type-M_2 Van Hove singularity which occurs at 1.72 THz in both the ir absorption and the perfect-crystal density of states.

Measurements of the absorption in KBr:H^- have been reported in Ref. 15 and by Ward and Timusk. Although the results of the two sets of measurements appear to differ rather significantly, common features are discernible. These may be summarized as follows: (i) a strong peak at ~2.67 THz attributed to a T_{1u} resonance, (ii) changes in slope at ~2.31, 2.49, and 2.61 THz, (iii) a sharp minimum, nearly reaching the base line, at ~2.28 THz and, in Ref. 19, a broad low-intensity band peaking at about 2.19 THz. Most of these features stand out prominently in the calculated curves of Fig. 6, and slight changes in slope can be discerned at ~2.34 and 2.64 THz. The T_{1u} resonance is slightly high in our calculations, coming at ~2.73 THz. It could be shifted by further changes in force constants, but since our value is probably within the combined errors of calculations and experiments, it seems acceptable to us.

The measurements of MacPherson and Timusk[15] on KI:H^- show three prominent peaks, at ~1.74, 1.83, and 1.92 THz. The calculations show a central peak at about 1.86 THz with a shoulder on each side which might be associated with the two peaks at 1.74 and 1.92 THz. However, the calculations also yield a sharp resonance at about 2.1 THz in the lower curve and a true localized gap mode at

about 2.2 THz in the upper curve. The experiments would certainly have picked this up if it actually existed apart from the three peaks. We conclude therefore that the resonance in our calculations is too high in frequency. However, attempts to push it to lower positions yielded about the same results as MacPherson and Timusk obtained in their parametrized calculations; i.e., the three-peaked nature of the experimental curve was lost. One feature of the calculated curve which was probably missed in the early experiments is the broad hump beginning at about 1.7 THz and extending to lower frequencies. As we have seen, a similar hump was found in the very recent measurements on KBr and it is likely that it would now also be found in KI.

We can summarize our impressions about the agreement between calculated and measured absorption curves as follows. The model and the calculations give the absorption in the sideband region in an entirely satisfactory manner when the obvious sources of disagreement are considered. The situation in the far-ir region is not quite as satisfactory. It is not clear at this time that the differences which do exist are entirely due to shortcomings in the model or in our calculations. In any case, it seem to us that the over-all agreement between the quantum-mechanical and the parametrized calculations is quite remarkable and that the agreement between theory and experiment is encouraging.

ACKNOWLEDGMENTS

We would like particularly to thank J. F. Cooke for his help with the Brillouin-zone integration schemes. We also wish to acknowledge useful discussions with M. Mostoller, T. Timusk, and M. V. Klein.

---

*Research sponsored by the U. S. Atomic Energy Commission under contract with Union Carbide Corporation, and by the Advanced Research Projects Agency under Contract No. HC 15-67-C-0221.

[1]J. H. Schulman and W. D. Compton, *Color Centers in Solids* (Pergamon, New York, 1962).

[2]G. Schaefer, J. Phys. Chem. Solid 2, 233 (1960).

[3]B. Fritz, in *Proceedings of* 1963 *International Conference on Lattice Dynamics*, edited by R. F. Wallis (Pergamon, London, 1964).

[4]A. J. Sievers, in *Low Temperature Physics*, edited by J. G. Daunt *et al.* (Plenum, New York, 1965), Vol. LT9, Pt. B; T. Timusk, E. J. Woll, Jr., and T. Gethins, in *Proceedings of the First International Conference on Localized Excitations in Solids*, edited by R. F. Wallis (Plenum, New York, 1968).

[5]I. M. Lifshitz, Nuovo Cimento Suppl. 3, 716 (1956) and references therein.

[6]G. F. Koster and J. C. Slater, Phys. Rev. 96, 1208 (1954) and references therein.

[7]R. Wallis and A. Maradudin, Progr. Theoret. Phys. (Kyoto) 24, 1055 (1960).

[8]S. Takeno, S. Kashirvamura, and E. Tenamoto, Progr. Theoret. Phys. Suppl. (Kyoto) 23, 124 (1962).

[9]S. S. Jaswal and D. J. Montgomery, Phys. Rev. 135, A1257 (1964).

[10]R. Fieschi, G. F. Nardelli, and N. Terzi, Phys. Rev. 138, A203 (1965).

[11]T. Timusk and M. V. Klein, Phys. Rev. 141, 664 (1966).

[12]J. B. Page, Jr. and B. G. Dick, Phys. Rev. 163, 910 (1967) and references therein.

[13]R. F. Wood and U. Öpik, Phys. Rev. 162, 736 (1967); R. F. Wood and R. L. Gilbert, Phys. Rev. 162, 746 (1967).

[14]J. F. Cooke and R. F. Wood, Phys. Rev. B 5, 1276 (1972).

[15]T. Gethins, T. Timusk, and E. J. Woll, Jr., Phys. Rev. 157, 744 (1967); R. W. MacPherson and T. Timusk, Can. J. Phys. 48, 2176 (1970); R. W. MacPherson and T. Timusk, Can. J. Phys. 48, 2917 (1970).

[16]M. V. Klein, in *Physics of Color Centers*, edited by W. Beall Fowler (Academic, New York, 1968), Chap. 7.

[17]M. P. Tosi and F. G. Fumi, J. Phys. Chem. Solids 25, 45 (1964).

[18]G. Gilat and L. J. Raubenheimer, Phys. Rev. 144, 390 (1966).

[19]R. W. Ward and T. Timusk, Phys. Rev. B (to be published). We wish to thank Professor Timusk for a preprint of this work.